Dalton Transactions

COMMUNICATION

View Article Online
View Journal | View Issue

Published on 20 April 2015. Downloaded by Michigan State University on 16/01/2016 12:20:53.

Cite this: *Dalton Trans.*, 2015, **44**, 9736

Received 13th March 2015,
Accepted 20th April 2015

DOI: 10.1039/c5dt01008j

www.rsc.org/dalton

The mechanism of hydrogen evolution in Cu(bztpen)-catalysed water reduction: a DFT study†

Rong-Zhen Liao,*[a] Mei Wang,[b] Licheng Sun[b,c] and Per E. M. Siegbahn*[d]

The mechanism of water reduction catalysed by a mononuclear copper complex Cu(bztpen) (bztpen = *N*-benzyl-*N*,*N*′,*N*′-tris(pyridine-2-ylmethyl)ethylenediamine) has been elucidated by DFT calculations, revealing that hydrogen evolution proceeds *via* coupling of a Cu(II)-hydride and a pendant pyridinium, and providing important implications for the future design of new catalytic systems for water reduction.

The sustainable production of clean fuels like molecular hydrogen has emerged as one of the major scientific challenges of this century.[1] Extraordinary efforts have been dedicated to the design of water reduction electrocatalysts that embrace only earth-abundant transition metals and exhibit a high turnover frequency (TOF) and turnover number (TON) with relatively low overpotentials. A variety of molecular electrocatalysts based on iron,[2] cobalt,[3] nickel,[4] and molybdenum[5] have been reported for hydrogen evolution in aqueous solutions. Very recently, Wang and co-workers reported the first mononuclear copper complex Cu^{II}(bztpen) that has been shown to act as a very efficient electrocatalyst for H_2 production in a phosphate buffer at pH 2.5 with an onset overpotential of 0.42 V.[6]

The crystal structure of $[Cu^{II}(bztpen)](BF_4)_2$ shows a distorted trigonal-bipyramidal coordination mode, in which a pyridine group and an amine group are situated at the axial positions.[6] Differential pulse voltammetry (DPV) measurement of the catalyst in phosphate buffer (pH = 2.5) showed a reversible peak at $E_{1/2}$ = −0.03 V, which was assigned to be a Cu^{II}/Cu^{I} redox process. This is followed by a water reduction catalytic peak at −0.82 V. Importantly, both reductions were found to be proton-coupled electron transfer (PCET) processes. With an applied potential of −0.60 V, the TOF was measured to be 1450 mol H_2 (mol cat)$^{-1}$ h^{-1} cm^{-2} (k_{obs} larger than 10 000 s^{-1}), with a TON of 2900 mol H_2 (mol cat)$^{-1}$ cm^{-2} in two hours. Two different mechanistic scenarios (Scheme 1) have been proposed for the hydrogen evolution. They differ mainly by where the proton enters upon the first reduction of Cu^{II} to Cu^{I}. If the proton goes to the metal, a Cu^{III}-hydride species is formed, or a Cu^{I}-pyridinium species is formed if the pyridine becomes protonated. The latter pathway appears to be more likely on the basis of UV/Vis and ^{1}H NMR spectroscopic studies.[6]

Inspired by this intriguing catalyst, we performed density functional calculations[7] at the B3LYP*-D3/SDD-6-311+G(2df,2p)//B3LYP/SDD-6-31G(d,p) level[8] to investigate the detailed redox processes and the H_2 formation mechanism. Our findings will provide important implications for the future design of new catalytic systems for electrocatalytic water reduction.

Our investigation starts from $[Cu^{II}(bztpen)]^{2+}$ (labelled as **1**), the optimized structure of which is shown in Fig. 1. Geometry optimization of **1** gave the Cu–N bonds in the range of 2.02–2.18 Å, which are in good agreement with the crystal structure (ranging from 1.99 to 2.13 Å).[6] In addition, overlay of

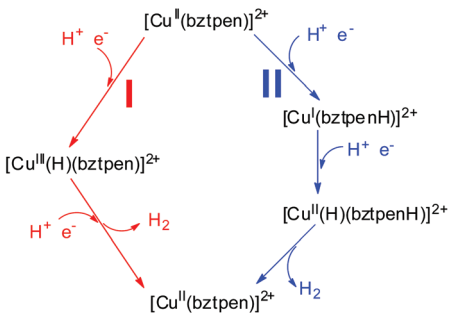

Scheme 1 Two possible pathways for H_2 production catalysed by $[Cu^{II}(bztpen)]^{2+}$.

[a]*Key Laboratory for Large-Format Battery Materials and System, Ministry of Education, School of Chemistry and Chemical Engineering, Huazhong University of Science and Technology, Wuhan 430074, China. E-mail: rongzhen@hust.edu.cn*
[b]*State Key Laboratory of Fine Chemicals, DUT-KTH Joint Education and Research Center on Molecular Devices, Dalian University of Technology (DUT), Dalian 116024, China*
[c]*Department of Chemistry, KTH Royal Institute of Technology, Stockholm 10044, Sweden*
[d]*Department of Organic Chemistry, Arrhenius Laboratory, Stockholm University, SE-10691 Stockholm, Sweden. E-mail: ps@organ.su.se*

†Electronic supplementary information (ESI) available: Computational details and coordinates for all structures. See DOI: 10.1039/c5dt01008j

This journal is © The Royal Society of Chemistry 2015

Published on 20 April 2015. Downloaded by Michigan State University on 16/01/2016 12:20:53.

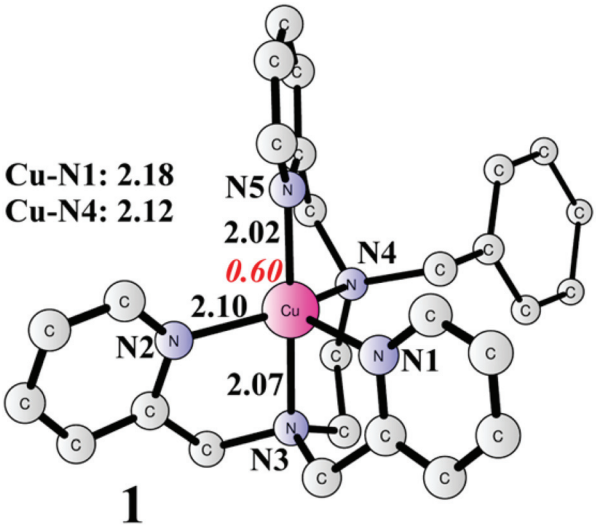

Fig. 1 Optimized structure of $[Cu^{II}(bztpen)]^{2+}$ (**1**). Distances are given in Ångstroms. The spin density on Cu is shown in red italic.

the optimized structure and the crystal structure gave a RMSD of 0.16 Å (see Fig. S1 in the ESI†). The spin state of **1** is a doublet and the spin density on Cu is 0.60 due to partial spin delocalization to the ligand. The pK_a of the protonated form $\mathbf{1_{pt}}$ (for structures of three isomers see Fig. S2 in the ESI†) is −1.5, suggesting that **1** is the major species in solution at pH 2.5.

At pH 2.5, the first reduction to generate a closed-shell singlet species **2** (Fig. 2) is a PCET process, in which the electron is added to reduce Cu^{II} to Cu^{I}, concomitant with the protonation of a pyridine group (pK_a of **2** is 6.0, the structure of the deprotonated form is shown in Fig. S3 in the ESI†). The reduction potential for the **2**/**1** couple was calculated to be −0.21 V, with a difference of 0.18 V compared with the experimental one.[6] Three different isomers ($\mathbf{2_A}$, $\mathbf{2_B}$, and $\mathbf{2_C}$) can be located, depending on whether the proton goes to N2, N1, or N5. The isomer $\mathbf{2_A}$ was calculated to be the most stable one, and the energies of $\mathbf{2_B}$ and $\mathbf{2_C}$ are 0.1 and 5.3 kcal mol^{-1} higher than that of $\mathbf{2_A}$, respectively. Interconversion between $\mathbf{2_A}$, $\mathbf{2_B}$, and $\mathbf{2_C}$ can easily take place, and the potential energy profile is shown in Fig. 3 (for the structures, see Fig. S4 in the ESI†). From $\mathbf{2_A}$ to $\mathbf{2_B}$, the barrier is only 9.6 kcal mol^{-1}, while it is 14.3 kcal mol^{-1} from $\mathbf{2_A}$ to $\mathbf{2_C}$. These results suggest that $\mathbf{2_A}$ and $\mathbf{2_B}$ are the dominant species and they are in a fast equilibrium. This is in very good agreement with the experimental ^{1}H NMR results, which suggest that two equivalent pyridine moieties are in a fast association/dissociation equilibrium.[6] Protonation of Cu^{I} to form a Cu^{III}-hydride intermediate (Fig. S5 and S6 in the ESI†) was also considered. The energy of this step is as high as 41.3 kcal mol^{-1} relative to the energy of $\mathbf{2_A}$. This is different from mononuclear Fe and Co-based catalysts, in which protonation of M^{I} (M = Fe or Co) is feasible to generate M^{III}-hydride.[9] Since the generation of Cu^{III}-hydride is thermodynamically very unfeasible, we can safely rule out pathway **I** in Scheme 1 as a viable option.

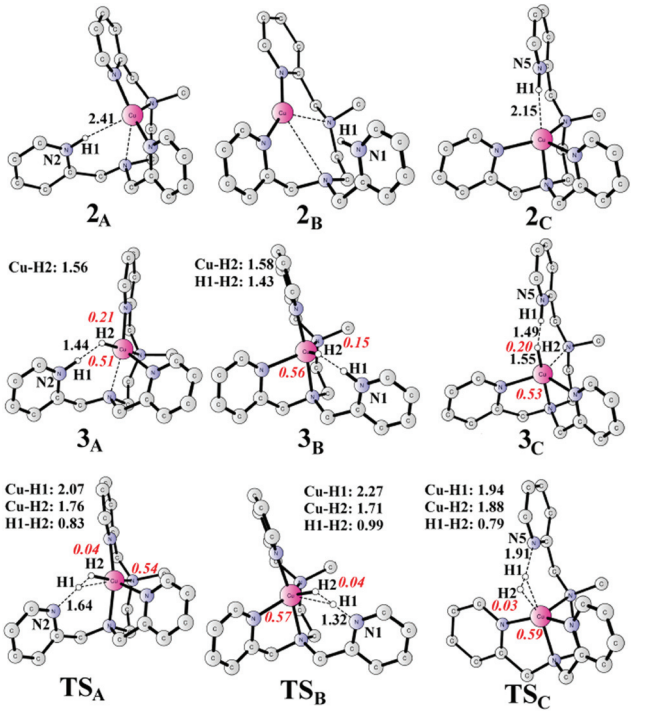

Fig. 2 Optimized isomers of **2** and **3**, and the H_2 formation transition state (**TS**). Distances are given in Ångstroms. For clarity, unimportant hydrogen atoms and the phenyl ring are not shown. Spin densities on Cu and H2 in **3** and **TS** are shown in red italic.

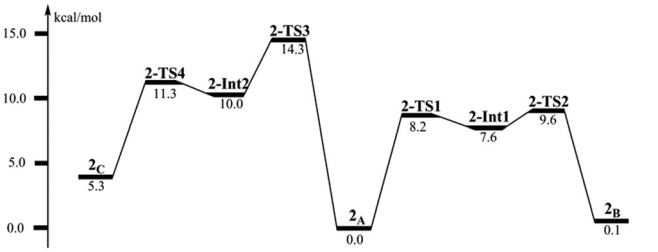

Fig. 3 Gibbs free energy profile for the interconversion of $\mathbf{2_A}$, $\mathbf{2_B}$, and $\mathbf{2_C}$.

Two alternative pathways to generate **2** from **1** have also been considered, namely proton transfer followed by electron transfer (PTET) and electron transfer followed by proton transfer (ETPT). For the PTET pathway, the protonation of **1** at pH 2.5 is endergonic by 5.5 kcal mol^{-1} (Fig. 4), and the following reduction has a potential of 0.03 V. For the ETPT pathway, the one electron reduction to generate $\mathbf{2_{dp}}$ has a potential of −0.64 V. In $\mathbf{2_{dp}}$, the Cu^{I} ion is penta-coordinated, and in order to make one of the pyridine ligands protonated, one pyridine ligand has to dissociate from the metal center to form $\mathbf{2_{dp'}}$ (for structures of three isomers see Fig. S3†). This process is endergonic by 3.1 kcal mol^{-1} (Fig. 4). When a potential of −0.6 V is applied, the formation of $\mathbf{2_{dp'}}$ from **1** is endergonic by 4.0 kcal mol^{-1}. These results are consistent with the experimental observation, which shows a PCET pathway.[6]

Published on 20 April 2015. Downloaded by Michigan State University on 16/01/2016 12:20:53.

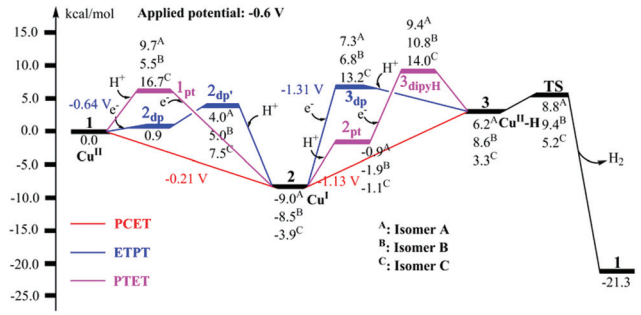

Fig. 4 Gibbs free energy diagram for the water reduction catalysed by **1**.

The subsequent reduction is also a PCET step with a potential of −1.13 V (experiment: −0.82 V) to generate a Cu^{II}-hydride intermediate **3** (pK_a = 5.1, the structures of the deprotonated forms are shown in Fig. S7 in the ESI†), with a doublet spin state. Consistently, three isomers were optimized. Unexpectedly, $\mathbf{3_C}$ has the lowest energy, while $\mathbf{3_A}$ and $\mathbf{3_B}$ lie +2.9 and +5.3 kcal mol^{-1} higher than **3c**, respectively. In $\mathbf{3_C}$, the Cu–H2 bond is 1.55 Å, the spin densities on Cu and H2 are 0.53 and 0.20, respectively. The distance between H1 and H2 is only 1.49 Å, suggesting the formation of an unconventional hydrogen bond,[10] and thus the hydride is ready for protonation to evolve H_2. It is also possible that the proton goes to a second pyridine group rather than the metal, thus generating a Cu^0 dipyridinium intermediate ($\mathbf{3_{dipyH}}$, Fig. S8 in the ESI†). However, the energy required to form the dipyridinium species is 6.1 kcal mol^{-1} higher than to form the Cu^{II}-hydride, suggesting that the generation of a Cu^{II}-hydride is preferred. This is also important for the following H–H bond formation, as the coupling of a Cu^{II}-hydride and a pendant pyridinium should be facile.

Similar to the **2**/**1** reduction, both ETPT and PTET pathways for the **3**/**2** reduction are thermodynamically less favourable (Fig. 4). For the ETPT pathway, the one electron reduction potential for $\mathbf{3_{dp}}$/**2** is −1.31 V, suggesting that the formation of $\mathbf{3_{dp}}$ is endergonic by 15.8 kcal mol^{-1} with an applied potential of −0.6 V. For the PTET pathway, the pK_a of $\mathbf{2_{pt}}$ (Fig. S9 in the ESI†) is calculated to be −2.7, implying that its formation is endergonic by 7.1 kcal mol^{-1} at pH 2.5. The following one electron reduction from $\mathbf{2_{pt}}$ to form $\mathbf{3_{dipyH}}$ has a potential of −1.09 V. Therefore, the formation of $\mathbf{3_{dipyH}}$ from **2** is endergonic by 18.4 kcal mol^{-1}. From a theoretical point of view, it is possible that the ETPT and/or PTET pathways are kinetically favoured even though they are thermodynamically less favoured. Modeling and calculation of the kinetics (transition state and rate) for such an electrochemical process, which involves electron transfer from the electrode to the catalyst, are very difficult. However, for the present case, the experimental results already suggested a PCET process for both the **2**/**1** and **3**/**2** reductions.[6]

The transition states (**TS**) for the H–H bond formation are optimized for each isomer and shown in Fig. 2. The $\mathbf{TS_C}$ has a barrier of only 1.9 kcal mol^{-1} relative to $\mathbf{3_C}$. If a potential of −0.6 V is applied (Fig. 4), the barrier of $\mathbf{TS_C}$ is 14.2 kcal mol^{-1} relative to $\mathbf{2_A}$, including an energetic penalty of 12.3 kcal mol^{-1} required for converting $\mathbf{2_A}$ to $\mathbf{3_C}$. However, the barrier for the interconversion between $\mathbf{2_A}$ and $\mathbf{2_C}$ is 14.3 kcal mol^{-1} (Fig. 3), which is almost the same as that for H_2 formation. Both transition states should thus contribute to the rate-limiting turnover of the catalyst. The H_2 formation *via* $\mathbf{TS_A}$ and $\mathbf{TS_B}$ is not preferred as their barriers are higher (17.8 and 18.4 kcal mol^{-1}, respectively). If a potential of −0.9 V is applied, the energy of $\mathbf{TS_C}$ becomes 7.3 kcal mol^{-1} relative to $\mathbf{2_A}$. This is lower than the barrier for the conversion of $\mathbf{2_A}$ to $\mathbf{2_C}$, which is required for the following H_2 formation step *via* $\mathbf{TS_C}$. Consequently, the conversion of $\mathbf{2_A}$ to $\mathbf{2_C}$ becomes rate-limiting and the total barrier is 14.3 kcal mol^{-1} for this pathway. However, the total barrier for $\mathbf{TS_A}$ in this case is only 10.9 kcal mol^{-1}, suggesting that there is no need for conversion of $\mathbf{2_A}$ to $\mathbf{2_C}$ and that H_2 formation proceeds *via* $\mathbf{TS_A}$ directly. The calculated barrier of 10.9 kcal mol^{-1} is consistent with the very large k_{obs} (larger than 10 000 s^{-1}) determined by experiment,[6] which can be converted into a barrier of about 10–11 kcal mol^{-1} using the classical transition state theory. It should be pointed out that the reduction of **2** to **3** might contribute to the rate-limiting turnover when a very negative potential is applied as the formation of H_2 is very fast. The nature of $\mathbf{TS_C}$ was confirmed to have only one imaginary frequency of 193.6*i* cm^{-1}, which corresponds to the H1–H2 bond formation. At $\mathbf{TS_C}$, the critical H1–H2, N5–H1, and Cu–H2 distances are 0.79, 1.91, and 1.88 Å, respectively. Downhill from $\mathbf{TS_C}$, H_2 dissociates from Cu to regenerate **1** and no stable Cu^{II}–H_2 adduct can be located, which was confirmed by IRC[11] calculations (Fig. S10 in the ESI†). In this mechanism, one of the three pyridine groups functions as a pendant base to take a proton during the first reduction, which reacts with the Cu^{II}-hydride created by the second reduction. This scenario also mimics the mechanism for the H–H bond formation/cleavage catalysed by [NiFe] and [FeFe]hydrogenase.[12] In addition, the critical role of a pendant base has been discussed by DFT calculations on a [FeFe]-hydrogenase model.[13]

In conclusion, we have investigated the mechanism for the [Cu^{II}(bztpen)]-catalysed water reduction. Both the experimentally-proposed pathways were examined, and the one with the involvement of a Cu^{III}-hydride as a key intermediate was ruled out due to its very high energy. The reaction starts with a PCET to generate a Cu^{I}-pyridinium intermediate, in which the proton can transfer between two pyridine groups in a fast equilibrium. The following PCET leads to the formation of a Cu^{II}-hydride intermediate, which is followed by H–H bond formation by coupling the Cu^{II}-hydride and the pyridinium group. The pendant pyridine group plays an important role in lowering the barrier for H_2 formation. H_2 release takes place directly after H–H bond formation, without the formation of a stable Cu^{II}–H_2 adduct. The total barrier for the H–H bond formation was calculated to be 14.3 kcal mol^{-1} with an applied potential of −0.6 V, and only 10.9 kcal mol^{-1} with an applied potential of −0.9 V. These findings provide a basis for the future design of copper-based water reduction electrocatalysts with high efficiency and low overpotential.

 This journal is © The Royal Society of Chemistry 2015

Published on 20 April 2015. Downloaded by Michigan State University on 16/01/2016 12:20:53.

This work was supported by startup funding from the Huazhong University of Science and Technology, the Swedish Research Council, and the Knut and Alice Wallenberg Foundation. The computer time was generously provided by the Swedish National Infrastructure for Computing.

Notes and references

1 J. A. Turner, *Science*, 2004, **305**, 972–974; T. R. Cook, D. K. Dogutan, S. Y. Reece, Y. Surendranath, T. S. Teets and D. G. Nocera, *Chem. Rev.*, 2010, **110**, 6474–6502.

2 (*a*) R. Mejia-Rodriguez, D. Chong, J. H. Reibenspies, M. P. Soriaga and M. Y. Darensbourg, *J. Am. Chem. Soc.*, 2004, **126**, 12004–12014; (*b*) Y. Na, M. Wang, K. Jin, R. Zhang and L. Sun, *J. Organomet. Chem.*, 2006, **691**, 5045–5051; (*c*) F. Quentel, G. Passard and F. Gloaguen, *Energy Environ. Sci.*, 2012, **5**, 7757–7761.

3 (*a*) B. D. Stubbert, J. C. Peters and H. B. Gray, *J. Am. Chem. Soc.*, 2011, **133**, 18070–18073; (*b*) Y. Sun, J. Sun, J. R. Long, P. Yang and C. J. Chang, *Chem. Sci.*, 2013, **4**, 118–124; (*c*) P. Zhang, F. Gloaguen and F. Quentel, *Chem. Commun.*, 2013, **49**, 9455–9457; (*d*) L. Chen, M. Wang, K. Han, P. Zhang, F. Gloaguen and L. Sun, *Energy Environ. Sci.*, 2014, **7**, 329–334.

4 (*a*) O. R. Luca, S. J. Konezny, J. D. Blakemore, D. M. Colosi, S. Saha, G. W. Brudvig, V. S. Bastista and R. H. Crabtree, *New J. Chem.*, 2012, **36**, 1149–1152; (*b*) P. Zhang, M. Wang, Y. Yang, D. Zheng, K. Han and L. Sun, *Chem. Commun.*, 2014, **50**, 14153–14156.

5 (*a*) H. I. Karunadasa, C. J. Chang and J. R. Long, *Nature*, 2010, **464**, 1329–1333; (*b*) H. I. Karunadasa, E. Montalvo, Y. Sun, M. Majda, J. R. Long and C. J. Chang, *Science*, 2012, **335**, 698–702.

6 P. Zhang, M. Wang, Y. Yang, T. Yao and L. Sun, *Angew. Chem., Int. Ed.*, 2014, **53**, 13803–13807.

7 For computational details, see the ESI.†

8 (*a*) A. D. Becke, *J. Chem. Phys.*, 1993, **98**, 5648–5652; (*b*) M. Reiher, O. Salomon and B. A. Hess, *Theor. Chem. Acc.*, 2001, **107**, 48–55.

9 (*a*) B. H. Solis and S. Hammes-Schiffer, *J. Am. Chem. Soc.*, 2011, **133**, 19036–19039; (*b*) B. H. Solis and S. Hammes-Schiffer, *Inorg. Chem.*, 2011, **50**, 11252–11262; (*c*) B. H. Solis and S. Hammes-Schiffer, *J. Am. Chem. Soc.*, 2012, **134**, 15253–15256; (*d*) B. H. Solis and S. Hammes-Schiffer, *Inorg. Chem.*, 2014, **53**, 6427–6443; (*e*) A. Bhattacharjee, E. S. Andreiadis, M. Chavarot-Kerlidou, M. Fontecave, M. J. Field and V. Artero, *Chem. – Eur. J.*, 2013, **19**, 15166–15174; (*f*) S. Kaur-Ghumaan, L. Schwartz, R. Lomoth, M. Stein and S. Ott, *Angew. Chem., Int. Ed.*, 2010, **49**, 8033–8036; (*g*) D. J. Graham and D. G. Nocera, *Organometallics*, 2014, **33**, 4994–5001.

10 R. H. Crabtree, P. E. M. Siegbahn, O. Eisenstein, A. L. Rheingold and T. F. Koetzle, *Acc. Chem. Res.*, 1996, **29**, 348–354.

11 C. Gonzalez and H. B. Schlegel, *J. Chem. Phys.*, 1989, **90**, 2154–2161.

12 P. E. M. Siegbahn, J. W. Tye and M. B. Hall, *Chem. Rev.*, 2007, **107**, 4414–4435.

13 (*a*) Y. Wang, M. Wang, L. Sun and M. S. G. Ahlquist, *Chem. Commun.*, 2012, **48**, 4450–4452; (*b*) Y. Wang and M. S. G. Ahlquist, *Dalton Trans.*, 2013, **42**, 7816–7822.